Three-body systems with Lagrange-mesh techniques in hyperspherical coordinates

P. Descouvemont and C. Daniel*
Physique Nucléaire Théorique et Physique Mathématique, CP229, Université Libre de Bruxelles, B-1050 Brussels, Belgium

D. Baye
Physique Quantique, CP165/82, Physique Nucléaire Théorique et Physique Mathématique, CP229, Université Libre de Bruxelles, B-1050 Brussels, Belgium

(Received 18 November 2002; published 28 April 2003)

We apply the Lagrange-mesh technique to three-body systems defined in hyperspherical coordinates. The method is applied to ^{6}He (described as $\alpha+n+n$) and ^{12}C (described as $\alpha+\alpha+\alpha$), and is shown to be fast and accurate. To deal with two-body forbidden states, we compare the usual projection method with the use of supersymmetric equivalent potentials. Both approaches provide similar spectroscopic properties, although the wave functions can be quite different. We also show that an accurate description of the three-body asymptotics requires bases with large hypermomenta.

DOI: 10.1103/PhysRevC.67.044309 PACS number(s): 21.60.Gx, 21.45.+v, 21.10.−k, 27.20.+n

I. INTRODUCTION

The hyperspherical coordinates and their main properties for three-particle systems are available for a long time [1]. The hyperspherical harmonics method (HHM) was first applied in the context of nuclear reactions by Delves [2] and the main tools of its mathematical formalism for three and more particles were derived by Smith [3,4]. The HHM allows transforming a many-body Schrödinger equation into a set of coupled differential equations depending on the single dimensional coordinate, the hyper-radius.

The HHM has a long story with many applications in atomic and nuclear physics [5,6]. In the following, we focus on three-body problems. Besides the important three-nucleon problem, the interest for the HHM has been renewed in nuclear physics with the discovery of halo nuclei with a two-neutron halo [7]. In first approximation, these systems can be treated as a three-body system composed of an inert core and of two ''halo'' neutrons. The accurate study of the bound state and continuum properties of these exotic nuclei is currently a problem of high interest.

A number of methods are able to treat three-body problems. In the HHM, the wave function is expanded in a series of hyperspherical harmonics, a complete basis set defined over a compact domain. The hyperspherical harmonics depend on four angles giving the spatial orientation of two Jacobi coordinates and one dimensionless variable related to their ratio, known as the hyperangle. With this expansion, an infinite system of coupled differential equations is obtained, which must be approximately solved with an appropriate truncation. In this system, matrix elements of the potential appear between hyperspherical harmonics. Calculating these matrix elements is rendered complicated by the fact that only one of the two-body relative coordinates appearing in the potential can enter the Jacobi-coordinate set, which serves to define the hyperspherical-coordinate system. Two types of approach can be chosen to solve this problem. Either the potential is expanded in multipoles [8] or the Jacobi coordinates undergo a pseudorotation that transforms the hyperspherical harmonics into another basis set [9]. As we are interested in a method where only numerical values of the potential should be used, we choose to apply the latter technique. One important advantage of the HHM is that forces depending on angular momentum, which are often encountered in nuclear physics, or three-body forces, can be treated without any modification of this approach.

In order to calculate bound-state wave functions and energies by solving the coupled hyperrradial equations, we employ the Lagrange-mesh method [10–14]. The Lagrange-mesh method is an approximate variational calculation that resembles a mesh calculation. This property is obtained by using a basis of Lagrange functions, i.e., indefinitely differentiable orthonormal functions that vanish at all points except one of an associated mesh. This basis corresponds to a truncation of a complete basis. The simplification comes from the use of the Gauss quadrature approximation corresponding to this mesh. Because of this Gauss quadrature, the potential matrix elements are replaced by their values at the mesh points. Strikingly, in spite of its simplicity, the Lagrange-mesh method appears to be as accurate as the corresponding variational calculation [14]. For the hyperradial coordinate, the selected Lagrange mesh involves the zeros of Laguerre polynomials and the Lagrange functions are regularized, i.e., multiplied by some power of the hyper-radius allowing a good representation of wave function properties near the origin [11,13]. The resulting method is mathematically equivalent to, but simpler than, a hyperspherical-harmonics calculation with an expansion based on Laguerre polynomials for the hyperradial coordinate. In order to establish the validity of the present approach, we compare it with a reference calculation performed with such a Laguerre basis, i.e., polynomials multiplied by a decreasing exponential. The calculation is performed in a numerically exact way.

The Lagrange-mesh method is illustrated with two examples. The first one is the ^{6}He halo nucleus described as a three-body system made up of an α particle and two neu-

*Present address: Optoelectronics Group, Cavendish Laboratory, Madingley Road, Cambridge CB3 0HE, United Kingdom.

trons. This physical example is interesting because of its small binding energy that implies a large spatial extension of the wave function and hence a slow convergence. It also raises the problem of the forbidden state that appears in each α-n subsystem, and which will be removed by two different techniques. The second example is the triple-α system, where each α is a pointlike boson interacting with the other ones through α-α effective forces. A 3α description of ^{12}C has been used by several authors, using different methods [15–17]. This problem is more academic because it does not provide an accurate description of the ''shell-model'' states of ^{12}C. However, it is well known [15,17] that this deficiency can be eliminated by using an appropriate three-body force to simulate nonlocal effects. In addition, it is interesting as a test because it involves several forbidden states for each subsystem, the Coulomb interaction, and full symmetrization. We also analyze the limits of validity of that model for the description of ^{12}C.

In Sec. II, the HHM is summarized. In Sec. III, the regularized Lagrange-mesh method based on Laguerre polynomials is described. Applications to ^{6}He and ^{12}C are presented and discussed in Sec. IV. Section V is devoted to the asymptotic properties of three-body wave functions. Concluding remarks are presented in Sec. VI.

II. THEORETICAL BACKGROUND

A. Hyperspherical formalism

The theory of the HHM is well known; we refer the reader to Refs. [9,7,18] for details. Here, we define the notation and present the basic properties of the hyperspherical formalism.

Let us consider three nuclei with mass numbers A_i (expressed in units of the nucleon mass m_N), and space coordinates $\boldsymbol{r}_i$. We define a set of Jacobi coordinates

$$\boldsymbol{x}_k=\sqrt{\mu_{ij}}(\boldsymbol{r}_j-\boldsymbol{r}_i),$$

$$\boldsymbol{y}_k=\sqrt{\mu_{(ij)k}}\left(\boldsymbol{r}_k-\frac{A_i\boldsymbol{r}_i+A_j\boldsymbol{r}_j}{A_i+A_j}\right), \tag{1}$$

where (i,j,k) is an even permutation of $(1,2,3)$, and where the (dimensionless) reduced masses are defined as

$$\mu_{ij}=A_iA_j/(A_i+A_j),$$

$$\mu_{(ij)k}=(A_i+A_j)A_k/(A_i+A_j+A_k). \tag{2}$$

Equations (1) define six coordinates that are transformed to the hyperspherical coordinates as

$$\rho^2=x_k^2+y_k^2,$$

$$\alpha_k=\arctan\frac{y_k}{x_k}, \tag{3}$$

where the hyper-radius ρ is independent of k, and where α_k varies between 0 and $\pi/2$. With the angular variables $\Omega_{x_k}=(\theta_{x_k},\varphi_{x_k})$ and $\Omega_{y_k}=(\theta_{y_k},\varphi_{y_k})$, Eqs. (3) define a set of hyperspherical coordinates, depending on k. This set of coordinates is known to be well adapted to the three-body Schrödinger equation.

Assuming two-body forces only, the Hamiltonian of the system is given by

$$H=\sum_{i=1}^{3}T_i+\sum_{i<j}V_{ij}(\boldsymbol{r}_j-\boldsymbol{r}_i), \tag{4}$$

where T_i is the kinetic energy of particle i, and V_{ij} a nucleus-nucleus interaction. For the sake of clarity, only the radial dependence is written. However, V_{ij} may also depend on other coordinates, such as momentum or spin (central and spin-orbit components are included in our applications). In the hyperspherical system, this Hamiltonian is rewritten as

$$H=T_{\text{c.m.}}+T_\rho+\sum_{i<j}V_{ij}\left(\frac{\boldsymbol{x}_k}{\sqrt{\mu_{ij}}}\right), \tag{5}$$

where $T_{\text{c.m.}}$ is the center of mass (c.m.) kinetic energy.

Let us define the set of angles

$$\Omega_{5i}=(\alpha_i,\Omega_{x_i},\Omega_{y_i}), \tag{6}$$

which enables us to rewrite the kinetic-energy term of Hamiltonian (5) as

$$T_\rho=-\frac{\hbar^2}{2m_N}\left(\frac{\partial^2}{\partial\rho^2}+\frac{5}{\rho}\frac{\partial}{\partial\rho}-\frac{K^2(\Omega_{5i})}{\rho^2}\right), \tag{7}$$

where K^2 is a five-dimensional angular momentum [3,9]. Its eigenfunctions, with eigenvalues $K(K+4)$, are the hyperspherical harmonics, and are written as

$$\mathcal{Y}^{\ell_x\ell_y}_{KLM_L}(\Omega_5)=\phi_K^{\ell_x\ell_y}(\alpha)[Y_{\ell_x}(\Omega_x)\otimes Y_{\ell_y}(\Omega_y)]^{LM_L}. \tag{8}$$

The quantum number K is the hypermomentum, and extends the concept of angular momentum to three-body systems [3]. The set of hyperspherical coordinates [i.e., the value of k in Eq. (1)] can be chosen freely. Here we will be dealing with systems involving a zero-spin core (generalization can be found in Ref. [20]), defined as particle 1. Hence the natural set of coordinates is $(\boldsymbol{x}_1,\boldsymbol{y}_1)$, and index $k=1$ will be dropped hereafter. In Eq. (8), we have [9]

$$\phi_K^{\ell_x\ell_y}(\alpha)=\mathcal{N}_K^{l_xl_y}(\cos\alpha)^{l_x}(\sin\alpha)^{l_y}P_n^{l_y+1/2,l_x+1/2}(\cos 2\alpha), \tag{9}$$

and the normalization factor $\mathcal{N}_K^{\ell_x\ell_y}$ is given by

$$\mathcal{N}_K^{l_xl_y}=\left[\frac{2n!(K+2)(n+l_x+l_y+1)!}{\Gamma\left(n+l_x+\frac{3}{2}\right)\Gamma\left(n+l_y+\frac{3}{2}\right)}\right]^{1/2},$$

$$n=\frac{K-\ell_x-\ell_y}{2}, \tag{10}$$

where n is a positive integer, and $P_n^{l_y+1/2,l_x+1/2}(x)$ is a Jacobi polynomial [21]. Introducing the spin component χ^{SM_S} yields the basis functions with total angular-momentum J,

$$\mathcal{Y}_{\gamma K}^{JM}(\Omega_5)=[\mathcal{Y}_{KL}^{\ell_x\ell_y}(\Omega_5)\otimes\chi^S]^{JM}, \tag{11}$$

where index γ stands for $(\ell_x\ell_y LS)$.

Wave functions (11) are used to expand the solution of the three-body Schrödinger equation

$$\left[T_\rho+\sum_{i<j}V_{ij}\left(\frac{\boldsymbol{x}_k}{\sqrt{\mu_{ij}}}\right)-E\right]\Psi^{JM\pi}=0, \tag{12}$$

as

$$\Psi^{JM\pi}(\rho,\Omega_5)=\rho^{-5/2}\sum_{\gamma K}\chi_{\gamma K}^{J\pi}(\rho)\mathcal{Y}_{\gamma K}^{JM}(\Omega_5), \tag{13}$$

where π is the parity, and where the radial wave functions $\chi_{\gamma K}^{J\pi}(\rho)$ are to be determined. The role of the $\rho^{-5/2}$ factor is to cancel out the first derivative in the kinetic energy (7). Next, expansion (13) is inserted in the Schrödinger equation (12), which leads to a set of coupled differential equations

$$\left[-\frac{\hbar^2}{2m_N}\left(\frac{d^2}{d\rho^2}-\frac{(K+3/2)(K+5/2)}{\rho^2}\right)-E\right]\chi_{\gamma K}^{J\pi}(\rho)+\sum_{K'\gamma'}V_{K'\gamma',K\gamma}^{J\pi}(\rho)\chi_{\gamma' K'}^{J\pi}(\rho)=0, \tag{14}$$

where the potential term is given by

$$V_{K'\gamma',K\gamma}^{J\pi}(\rho)=V_{K'\gamma',K\gamma}^{J\pi(1)}(\rho)+V_{K'\gamma',K\gamma}^{J\pi(2)}(\rho)+V_{K'\gamma',K\gamma}^{J\pi(3)}(\rho). \tag{15}$$

Since coordinate $\boldsymbol{x}_1$ is adapted to the first term, it is determined directly as

$$V_{K'\gamma',K\gamma}^{J\pi(1)}(\rho)=\int\mathcal{Y}_{\gamma' K'}^{JM*}(\Omega_5)V_{23}\left(\frac{\rho\cos\alpha}{\sqrt{\mu_{23}}}\right)\mathcal{Y}_{\gamma K}^{JM}(\Omega_5)d\Omega_5. \tag{16}$$

The second and third terms are first determined in the $\boldsymbol{x}_2$ and $\boldsymbol{x}_3$ coordinate systems, and then transformed to the $\boldsymbol{x}_1$ system with the Raynal-Revai coefficients $\langle\ell_x'\ell_y'|\ell_x\ell_y\rangle_{KL}$ [9]. We have

$$\mathcal{Y}_{KLM_L}^{\ell_x\ell_y}(\Omega_{5j})=\sum_{\ell_x'\ell_y'}\langle\ell_x'\ell_y'|\ell_x\ell_y\rangle_{KL}\mathcal{Y}_{KLM_L}^{\ell_x'\ell_y'}(\Omega_5). \tag{17}$$

In practice, the integrations over Ω_x and Ω_y are performed analytically, whereas integration over α is carried out numerically with the Gauss-Legendre approximation. For large ρ values, matrix elements of the potential vary rapidly with the hyperangle α. Typically, we use 60 points for the Gauss-Legendre quadrature, which provides a very good accuracy for all considered ρ values.

The parity of the system is given by

$$\pi=\pi_1\pi_2\pi_3(-1)^{\ell_x+\ell_y}=\pi_1\pi_2\pi_3(-1)^K, \tag{18}$$

where π_i is the parity of particle i. If particles 2 and 3 are identical, we have the selection rule

$$(-1)^{\ell_x+S+T}=-1, \tag{19}$$

S and T being the total spin and isospin of the system composed by these particles. In this case, partial waves which do not satisfy Eq. (19) are removed from the basis. For ^{12}C, all particles are identical, which means that the wave function must be invariant for any particle permutation. In other words the wave function must be replaced by its symmetric form

$$\Psi^{JM\pi}(\rho,\Omega_5)\rightarrow\Psi^{JM\pi}(\rho,\Omega_{5,1})+\Psi^{JM\pi}(\rho,\Omega_{5,2})+\Psi^{JM\pi}(\rho,\Omega_{5,3}), \tag{20}$$

and the wave function is symmetrized through further Raynal-Revai transformations.

B. Removal of Pauli forbidden states

In microscopic cluster models, where antisymmetrization between all nucleons is taken into account, the existence of forbidden states in nucleus-nucleus systems is well established [22,23]. The role of forbidden states can be simulated by additional (unphysical) states in the nucleus-nucleus potential [23]. In two-body systems, these additional states are not considered for investigating properties of the system. However, for three-body systems, a special treatment is necessary to remove forbidden states, as they would introduce unphysical eigenvalues of the Hamiltonian. The effect of Pauli blocking in three-body models has been addressed in detail by Thompson *et al.* [18], who investigate different techniques to remove two-body forbidden states.

Here, we consider two methods to deal with forbidden states: (i) the projection technique [24] and (ii) a supersymmetric transform of the nucleus-nucleus potential [25]. In the projection method, the nucleus-nucleus potential $V_{ij}(\boldsymbol{x})$ is replaced by

$$V_{ij}(\boldsymbol{x})\rightarrow V_{ij}(\boldsymbol{x})+\Lambda\sum_f|\psi_f(\boldsymbol{x})\rangle\langle\psi_f(\boldsymbol{x})|, \tag{21}$$

where f runs over all two-body forbidden-states $\psi_f(\boldsymbol{x})$; in particular, it may include different angular momenta. In Eq. (21), Λ is a constant energy, taken much larger than the characteristic energies of the system (typically $\Lambda\sim10^5-10^9$ MeV). The role of the projector in Eq. (21) is to move the forbidden states up to very high energies. The final results must be, up to the accuracy of the model, insensitive to the choice of Λ.

The second method considered here is to replace potential $V_{ij}(x)$ by its supersymmetric partner

$$V_{ij}(\boldsymbol{x})\rightarrow\tilde{V}_{ij}(\boldsymbol{x}). \tag{22}$$

Potential $\tilde{V}_{ij}(x)$ is phase equivalent to $V_{ij}(x)$, i.e., the phase shifts are identical, but does not contain unphysical states.

The role of forbidden states is simulated by a short-range repulsive core. As long as scattering cross sections are concerned, $V_{ij}(x)$ and $\tilde{V}_{ij}(x)$ provide identical results. However, the associated wave functions are different since supersymmetric wave functions do not present nodes corresponding to the forbidden states. The study of three-body systems therefore offers a good opportunity to analyze the differences between both approaches.

III. LAGRANGE-MESH TECHNIQUES WITH HYPERSPHERICAL COORDINATES

A. General definitions

In the preceding section the coordinate ρ denotes a hyperradius and x a relative coordinate between two particles. In order to treat them simultaneously, the coordinate in the present section is denoted as u.

A Lagrange basis [10] is defined in relation with a set of N mesh points $u_i \in (0,\infty)$, called a Lagrange mesh. The Lagrange functions are N orthonormal functions $f_i(u)$ verifying at the N mesh points u_i the Lagrange conditions

$$f_i(u_{i'}) = \lambda_i^{-1/2} \delta_{ii'}, \tag{23}$$

i.e., each function $f_i(u)$ vanishes at all mesh points except at u_i. The constants λ_i appearing in Eq. (23) are the weights of the Gauss quadrature approximation associated with the mesh,

$$\int_0^\infty g(u)du \approx \sum_{k=1}^{N} \lambda_k g(u_k). \tag{24}$$

As a result of the Lagrange conditions (23), the basis functions $f_i(u)$ are orthogonal at the Gauss approximation. They are even exactly orthonormal when the Gauss quadrature is exact for products of Lagrange functions,

$$\int_0^\infty f_i(u) f_{i'}(u) du = \delta_{ii'}. \tag{25}$$

This is, for example, the case when Lagrange functions are constructed from orthogonal polynomials [10].

The Gauss approximation is applied to the potential matrix elements. The approximate potential matrix is then diagonal,

$$\int_0^\infty f_i(u) V(u) f_{i'}(u) du \approx V(u_i) \delta_{ii'}. \tag{26}$$

The kinetic-energy matrix elements of the operator $-d^2/du^2$ can also be calculated at the Gauss approximation as

$$T^G_{ii'} = -\lambda_i^{1/2} f''_{i'}(u_i). \tag{27}$$

The resulting expressions only depend on the u_i and $u_{i'}$, but are not necessarily symmetric.

Let us first define the Lagrange-Laguerre basis

$$f_i(u) = (-1)^i u_i^{1/2} \frac{L_N(u)}{u-u_i} e^{-u/2}, \tag{28}$$

where $L_N(u)$ is a Laguerre polynomial, and where the mesh points u_1 to u_N are given by

$$L_N(u_i) = 0. \tag{29}$$

The Gauss-Laguerre quadrature is then obtained with the weights [21]

$$\lambda_i = \frac{e^{u_i}}{u_i [L'_N(u_i)]^2}. \tag{30}$$

The basis (28) is however not interesting here because the basis functions do not behave properly at small distances.

Therefore, we introduce a regularization factor [11,12] which can be fitted to each case. We consider the Lagrange-Laguerre basis defined by

$$\hat{f}_i(u) = \left(\frac{u}{u_i}\right)^n f_i(u), \tag{31}$$

with u_i given by Eq. (29). This basis is not exactly orthogonal but is still orthogonal at the Gauss approximation. Notice that the Lagrange condition (23) is still satisfied.

The Gauss approximation $\hat{T}^G_{ii'} = -\lambda_i^{1/2} \hat{f}''_{i'}(u_i)$ for the kinetic-energy matrix elements leads after a straightforward calculation to

$$\hat{T}^G_{ii} = (12u_i^2)^{-1}[-12n^2+24n-8+(4N+2)u_i-u_i^2] \tag{32}$$

and, for $i \neq i'$,

$$\hat{T}^G_{ii'} = (-1)^{i-i'} \frac{u_{i'}^{n-3/2}}{u_i^{n-1/2}} \frac{(2n-3)u_{i'}-(2n-1)u_i}{(u_i-u_{i'})^2}. \tag{33}$$

At the Gauss approximation, the centrifugal term is given for any n by

$$\int_0^\infty \hat{f}_i(u) u^{-2} \hat{f}_{i'}(u) du \approx u_i^{-2} \delta_{ii'}, \tag{34}$$

which is exact for $n \leqslant 3/2$. We shall make use of Eqs. (31) to (34) in two particular cases.

Near the origin $r=0$, two-body relative wave functions behave as r^{l+1}, where l is the relative orbital momentum. This behavior is well simulated by an expansion in basis functions (31) with $n=1$ [13,14]. Indeed, this basis is exactly equivalent to a set of Laguerre polynomials multiplied by $u\exp(-u/2)$, whose linear combinations are able to reproduce u^{l+1} for small u provided that the basis size N is large enough, i.e., larger than l.

The functions of the hyper-radius $\chi^{J\pi}_{\gamma K}(\rho)$ behave near the origin as $\rho^{K+5/2}$, which cannot be reproduced with a combination of polynomials. Hence, in this case, we use the $n=3/2$ regularization. The basis is then exactly equivalent to a set of Laguerre polynomials multiplied by $u^{3/2}\exp(-u/2)$.

Linear combinations of these basis functions are able to reproduce a $u^{K+5/2}$ behavior for small u provided that the basis size N is large enough, i.e., larger than $K+1$. The choice $n=5/2$ might seem more obvious but for this value the matrix $\hat{T}^G$ is not symmetric. It is thus preferable to choose $n=3/2$. For $n=3/2$ as well as for $n=1$, the kinetic-energy matrix is symmetric at the Gauss approximation. Moreover, the centrifugal matrix elements (34) are exact. This would not be true for $n>3/2$.

For $n=3/2$, the exact overlaps are given by

$$\int_0^\infty \hat{f}_i(u)\hat{f}_{i'}(u)du=\delta_{ii'}+(-1)^{i-i'}\frac{2N+1+u_i+u_{i'}}{u_i u_{i'}}. \tag{35}$$

The exact kinetic-energy matrix elements read

$$\hat{T}_{ii'}=\hat{T}^G_{ii'}+(-1)^{i-i'}\frac{2N+1-u_i-u_{i'}}{4u_i u_{i'}}. \tag{36}$$

Equations (35) and (36) are rather easily established with the technique explained in the appendix of Ref. [11]. For $n=1$, the exact overlaps and kinetic-energy matrix elements $\hat{T}_{ii'}$ are given in Refs. [11,14].

B. Matrix elements

Let us expand the hyperradial functions $\chi^{J\pi}_{\gamma K}(\rho)$ in the Lagrange basis as

$$\chi^{J\pi}_{\gamma K}(\rho)=h^{-1/2}\sum_{i=1}^{N} C^{J\pi}_{\gamma Ki}\hat{f}_i(\rho/h), \tag{37}$$

where N is the number of Lagrange functions, and h a scaling parameter that should be optimized according to the physics of the problem. When N is large enough, the sensitivity with respect to h should be negligible. In practice, this scaling parameter is used to reduce the number of basis states. Numerical examples will be shown in the following section. Inserting expansion (37) in the Schrödinger equation (12) provides

$$\sum_{\gamma' K' i'}(H^{J\pi}_{\gamma Ki,\gamma' K' i'}-E\,\delta_{\gamma\gamma'}\delta_{KK'}\delta_{ii'})C^{J\pi}_{\gamma' K' i'}=0, \tag{38}$$

where matrix $\boldsymbol{H}^{J\pi}$ reads

$$H^{J\pi}_{\gamma Ki,\gamma' K' i'}=\frac{\hbar^2}{2m_N}\left[\frac{1}{h^2}\hat{T}^G_{ii'}+\frac{(K+3/2)(K+5/2)}{x_i^2}\delta_{ii'}\right]\delta_{\gamma\gamma'}\delta_{KK'}+V^{J\pi}_{\gamma K,\gamma' K'}(x_i)\delta_{ii'} \tag{39}$$

with $x_i=hu_i$. In this definition, the kinetic-energy matrix elements are given by Eqs. (32) and (33). Matrix elements of the potential term are computed according to Eq. (15) and, after integration over angle α, involve the potential at the mesh points only; they are diagonal with respect to i.

C. Treatment of forbidden states

As mentioned before, Pauli forbidden states are accounted for in two ways. Using a supersymmetric transformation to the nucleus-nucleus potentials in quite simple: V_{23} in Eq. (16) is replaced by $\tilde{V}_{23}$ as explained in Sec. II B. The treatment of the Pauli projection is more tedious, and is outlined in this section.

The projector involved in Eq. (21) explicitly depends on coordinate $\boldsymbol{x}$; accordingly the basis wave functions should be expressed in system $(\boldsymbol{x},\boldsymbol{y})$ in place of (ρ,Ω_5). Let us define

$$\tilde{\Phi}^{JM\pi}_{\gamma Ki}(\boldsymbol{x},\boldsymbol{y})=\mathcal{Y}^{JM}_{\gamma K}(\Omega_5)\hat{f}_i(\rho/h), \tag{40}$$

and introduce the projector

$$P=\sum_{\ell j} P_{\ell j}, \tag{41}$$

where $P_{\ell j}$ is given by

$$P_{\ell j}=\sum_m |\psi^{\ell sj}(x)Y^{\ell sjm}(\Omega_x)\rangle\langle\psi^{\ell sj}(x)Y^{\ell sjm}(\Omega_x)|. \tag{42}$$

In this definition, $\psi^{\ell sj}(x)$ is the radial part of the Pauli forbidden states; we do not explicitly write index f. Angular functions $Y^{\ell sjm}(\Omega_x)$ are given by

$$Y^{\ell sjm}(\Omega_x)=[Y_\ell(\Omega_x)\otimes\chi^s]^{jm}, \tag{43}$$

χ^s being a spinor with spin s. The radial part is expanded over a set of Lagrange functions $\hat{g}_i(x/h_2)$ as

$$\psi^{\ell sj}(x)=h_2^{-1/2}\sum_{k=1}^{N_2} D_k^{\ell sj}\hat{g}_k(x/h_2), \tag{44}$$

where N_2 and h_2 are the number of functions and the scale factor adapted to the two-body problem. According to the discussion of Sec. III A, $\hat{g}_k$ are Lagrange functions defined with $n=1$. We, therefore, introduce two different Lagrange meshes: one for the three-body wave functions and another for the two-body forbidden states. Since the projector $P_{\ell j}$ is multiplied by a large constant Λ, slight numerical inaccuracies in the two-body forbidden states are amplified. A precise description of the $\psi^{\ell sj}(x)$ function is therefore required. Using a Lagrange expansion for the forbidden states is not necessary, but enables us to simplify integrals involving those wave functions. Technical details are given in Appendix A.

IV. APPLICATION TO ^{6}He AND ^{12}C

A. Conditions of the calculations

Here we apply the Lagrange-mesh technique to two systems: (i) the ^{6}He nucleus is a well-established three-body system with a low binding energy, which has been studied by

TABLE I. Energies and rms radii of ^{6}He and ^{12}C. $\sqrt{\langle r^2\rangle}$ is obtained with 1.47 fm for the α-particle radius.

	Projection		Supersymmetry	
^{6}He	$\lambda=1$	$\lambda=1.0044$	$\lambda=1$	$\lambda=1.027$
E(MeV)	-0.87	-0.97	-0.38	-0.97
$\sqrt{\langle\rho^2\rangle}$ (fm)	5.20	5.11	5.72	5.21
$\sqrt{\langle r^2\rangle}$ (fm)	2.44	2.41	2.63	2.44
^{12}C	$\lambda=1$	$\lambda=1.096$	$\lambda=1$	$\lambda=1.088$
E(MeV)	-0.26	-7.29	-1.01	-7.29
$\sqrt{\langle\rho^2\rangle}$ (fm)	8.24	6.36	8.24	6.84
$\sqrt{\langle r^2\rangle}$ (fm)	2.80	2.35	2.80	2.46

many authors; (ii) the ^{12}C nucleus is strongly bound with respect to the 3α threshold (-7.27 MeV) and therefore should be considered as a compact system. The aim of the next sections is to illustrate the Lagrange-mesh technique and to discuss its numerical accuracy. Only bound states of ^{6}He and ^{12}C will be considered. We use $\hbar^2/2$ amu $=20.9008$ MeV fm^2, $m_\alpha=4.0026$ amu and $m_N=1.0087$ amu.

For ^{6}He the α-neutron potential $V_{\alpha n}$ is taken from Kanada *et al.* [26]. This potential contains one forbidden state for $\ell=0$. The n-n potential is chosen as the Minnesota interaction [27]. For the α-α potential, used for ^{12}C, we adopt the force derived by Buck *et al.* [23], which accurately reproduces the α-α phase shifts up to 20 MeV. This ℓ-independent potential involves two forbidden states for $\ell=0$, and one for $\ell=2$. The screened Coulomb interaction is a point-sphere function, used according to Ref. [23].

B. Accuracy of the Lagrange-mesh method

The main parameters in the method are the number of functions N and the scale parameter h. The results should be independent of their values, but they can be optimized to deal with bases as small as possible. As it is well known [18], three-body calculations underpredict the binding energies. For halo nuclei, the wave function sensitively depends on the binding energy, and a correction to the potential must be performed to reproduce the three-body state.

First, calculations are performed with $N=30$ and $h=0.3$ fm (typical values of N_2 and h_2 are similar). We use $K_{max}=24$ and 30 for ^{6}He and ^{12}C, respectively. Energies and radii are given in Table I. The rms radius $\sqrt{\langle r^2\rangle}$ is calculated from the $\sqrt{\langle\rho^2\rangle}$ expectation value by assuming the α-particle radius $\sqrt{\langle r^2\rangle_\alpha}=1.47$ fm [19].

For ^{6}He, the renormalization factor λ of the α-n interaction is very close to unity, as expected for a Borromean system, where the three particles are located far from each other. For $\lambda=1$, the obtained energy -0.87 MeV is close but not identical to the value -0.73 MeV obtained in Ref. [13], under exactly the same model conditions. The reason of the difference lies in the angular-momentum dependence of the α-n potentials, which is not treated exactly when the core-nucleon system of coordinates is employed, as in Ref. [13]. It is not due to the Lagrange-mesh approximation that is used in both works for different coordinates. This can easily be checked by dropping any angular-momentum dependence in both calculations. Then the converged results coincide.

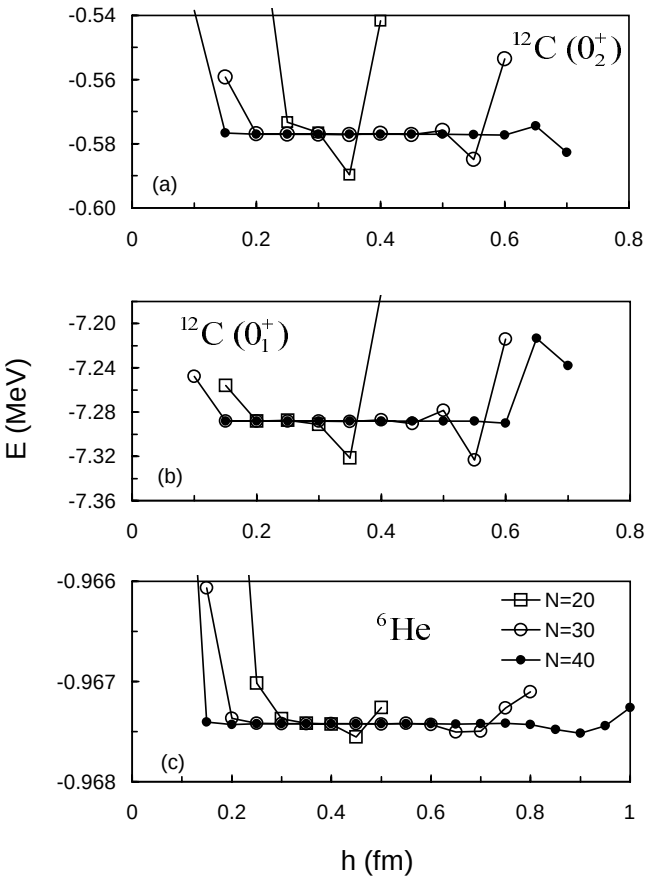

FIG. 1. Energies of ^{12}C (0_2^+) (a), ^{12}C (g.s.) (b), and ^{6}He (c) with respect to the three-particle threshold versus the Lagrange parameters N and h. The projection method is used to remove two-body forbidden states.

For ^{12}C, the α-α potential must be renormalized by a larger factor λ to reproduce the experimental binding energy. This is not surprising for a compact system where nonlocal effects are expected to play a role. Notice that this procedure affects the two-body asymptotics since ^{8}Be is slightly bound with $\lambda=1.096$. This problem can be avoided by introducing a three-body force [17,18], which will be discussed in Sec. V B. Without renormalization, the ^{6}He energy is higher with supersymmetry than with the projection method, whereas the situation is reversed for ^{12}C. Qualitatively, both techniques of forbidden-state removal yield similar results: the energies and rms radii do not differ significantly. In Fig. 1, we illustrate the accuracy of the Lagrange-mesh method with different N and h values. As expected [10], a plateau occurs, which here is located around $h=0.3$ fm for ^{12}C and $h=0.4$ fm for ^{6}He. This plateau gets broader when the number of functions N increases, $N=40$ provides a wide range of acceptable h values. The size of the basis can be reduced to $N=30$ without any loss of accuracy. Notice that, when the accuracy is poor, the energy can be *below* the correct values (see, for example, values for $N=20$). This is not possible in exact variational calculations, but appears here from the Gauss ap-

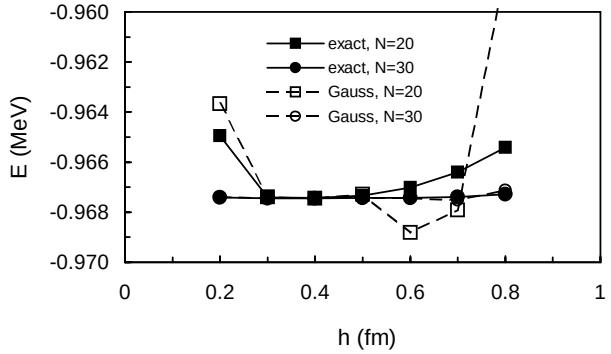

FIG. 2. ^{6}He binding energy as a function of the mesh size h, with the exact calculation (full symbols) and with the Gauss approximation (open symbols). For $N=30$, the exact and approximate results are almost superimposed.

proximation used to compute the matrix elements.

To test the validity of the Gauss approximation, we have calculated the ^{6}He binding energy *without* this approximation. The overlap and kinetic energy are calculated with Eqs. (35) and (36), respectively; the potential matrix elements are obtained from an accurate numerical integration over the hyper-radius. The results, which correspond to an exact variational calculation, are presented in Fig. 2. Near the variational minimum ($h\approx 0.4$ fm), the Gauss approximation is accurate within 10^{-6}. With $N=30$, the differences are insignificant in a wide range of h values. As expected, the validity of the Gauss approximation is more limited for $N=20$. Notice that the exact variational calculation requires much longer computer times. The matrix is not anymore diagonal, and each matrix element is an integral, in place of a single evaluation of the potential at the mesh points. In addition the overlap matrix is not unity, which may raise accuracy problems. For large bases, the increase of computer times is at least a factor of 10.

Figure 3 shows the convergence with respect to K_{max} of the 0^+ states in ^{6}He and ^{12}C, including the 0_2^+ excited state of ^{12}C. Since ^{6}He contains a spin-orbit component, the number of basis functions N_{max} [in other words, the number of γK values in Eq. (13)] increases quickly with K_{max}. We have as follows:

$$\begin{aligned} N_{max} &= (K_{max}+2)(K_{max}+4)/8 \quad \text{for } {}^6\text{He} \\ &= (K_{max}+4)^2/16 \quad \text{for } {}^{12}\text{C } (K_{max}/2 \text{ even}) \\ &= (K_{max}+2)(K_{max}+6)/16 \quad \text{for } {}^{12}\text{C } (K_{max}/2 \text{ odd}). \end{aligned} \tag{45}$$

For the largest K_{max} considered here ($K_{max}=24$ for ^{6}He, $K_{max}=30$ for ^{12}C), we have $N_{max}=91$ and $N_{max}=72$, respectively. These values are quite reasonable to have a good convergence, but are not optimized for the 0_2^+ state of ^{12}C which would require K_{max} significantly larger than 30. The rms radii, illustrated in the lower panel of Fig. 3 reach convergence for rather low values of K_{max}; for both systems $K_{max}=12$ provides the rms radii with an accuracy better than 1%.

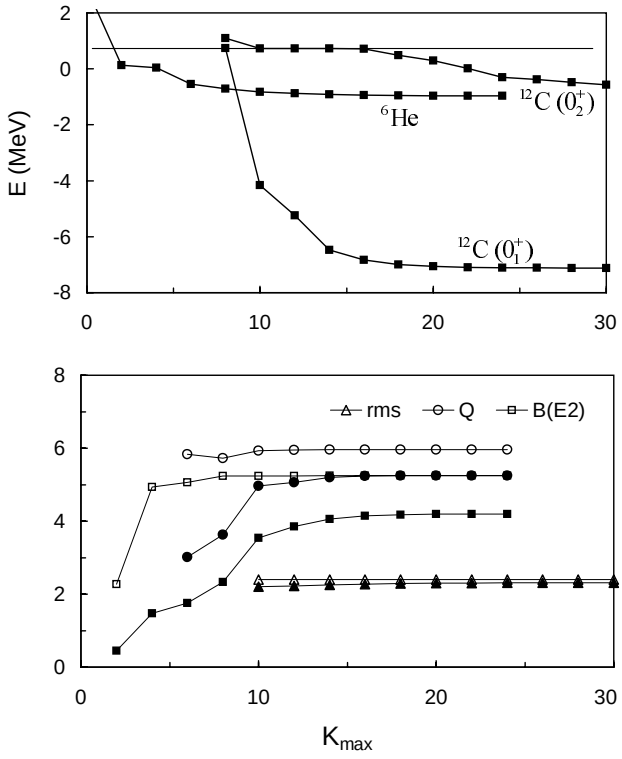

FIG. 3. Convergence of the energy (upper panel) and of the rms radius, $Q(2^+)$ and $B(E2,2^+\rightarrow 0^+)$ in ^{12}C (lower panel) with respect to K_{max}. Quadrupole moments, rms radii, and $B(E2)$ values are given in e fm^2, fm, and Wu, respectively.

As mentioned before, one of our aims is to compare two methods to remove forbidden states. The projection technique does not affect the nucleus-nucleus potential, but introduces nonlocality in the three-body Hamiltonian. In Fig. 4, we display the convergence versus the projection amplitude Λ. Since ^{6}He contains one forbidden state in both α-n potentials, the convergence is reached with rather low Λ values. Conversely, the α-α potential involves three forbidden states which makes projector (21) quite complicated. In such case, very accurate numerical conditions are required. In particular the α-α forbidden states must be described with a high accuracy [28].

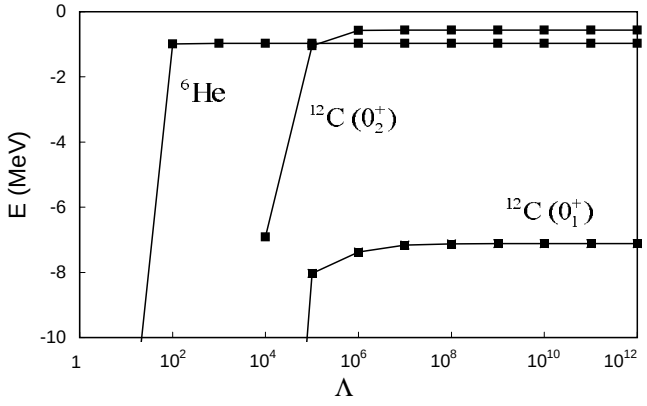

FIG. 4. Convergence of the energy with respect to the projection amplitude Λ.

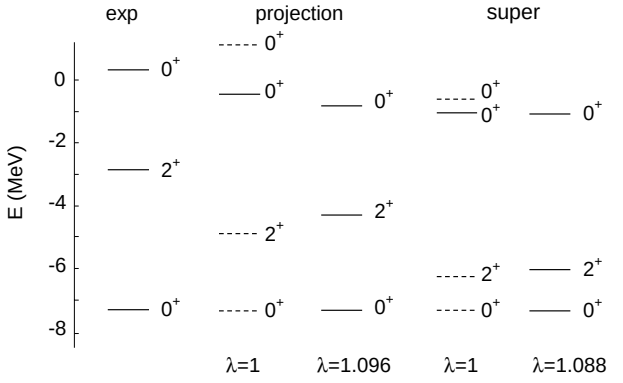

FIG. 5. Energy spectrum of ^{12}C with and without renormalization factors. Energies are given with respect to the 3α threshold. Dashed lines correspond to the use of a three-body force.

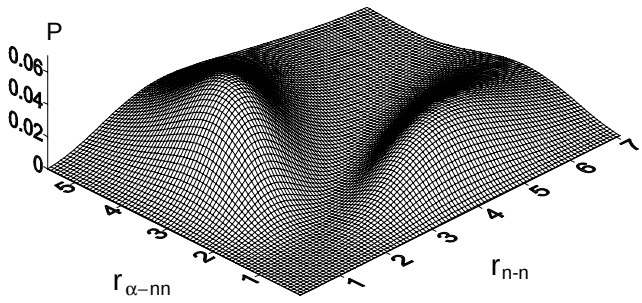

FIG. 6. ^{6}He probability P [see Eq. (46)] for the $S=0$ component. Distances are given in fm.

C. Spectra and wave functions

The spectrum of ^{12}C is illustrated in Fig. 5. With the nonrenormalized α-α potential ($\lambda=1$) the ground-state energy is far from experiment [29]. Introducing the renormalization factors given in Table I provides more realistic energies although the spectra are too compressed. Further tests of the wave functions will be provided by electromagnetic transition probabilities (see Sec. IV D).

The ^{6}He and ^{12}C wave functions are plotted in Figs. 6 and 7, respectively. The probability $P(x,y)$ is defined as

$$P^{J\pi}(x,y)=\int d\Omega_x d\Omega_y |\Psi^{JM\pi}(\boldsymbol{x},\boldsymbol{y})|^2, \tag{46}$$

which is plotted as a function of the relative coordinates ($r_{n-n}=\sqrt{2}x$ and $r_{\alpha\text{-}nn}=\sqrt{3/4}y$ for ^{6}He, and $r_{\alpha\text{-}\alpha}=x/\sqrt{2}$ and $r_{\alpha\text{-}\alpha\alpha}=\sqrt{2/3}y$ for ^{12}C).

For ^{6}He, we obtain the well known wave function, with two maxima. This wave function is similar to the wave function obtained by Voronchev *et al.* [30] who find a maximum at large $r_{\alpha\text{-}nn}$ values (''dineutron'' configuration), and one at large r_{nn} values (''cigar'' configuration). The amplitude of the first maximum is larger by about 50%.

Both methods of forbidden-state removal provide very similar wave functions, and would be undistinguishable at the scale of the figure. The situation is different for ^{12}C (Fig. 7), where the projection technique is responsible for several node lines in the wave function; in particular, the 0_2^+ wave

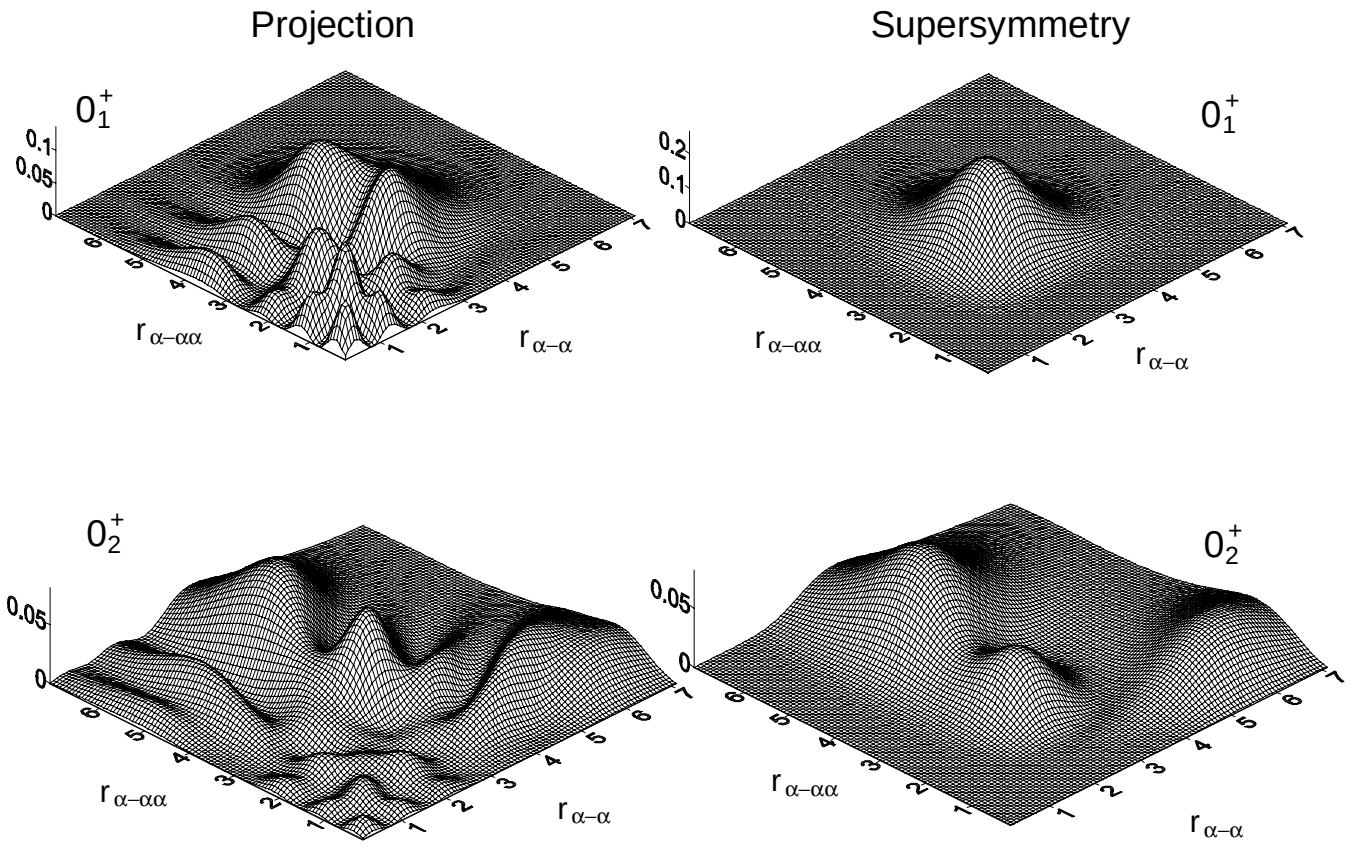

FIG. 7. ^{12}C probability P [see Eq. (46)] for the ground and 0_2^+ states. Distances are given in fm.

TABLE II. Weights of K components in ^{6}He and ^{12}C.

K	^{6}He		^{12}C (0_1^+)		^{12}C (0_2^+)	
	Projection	Super.	Projection	Super.	Projection	Super.
0	3.64×10^{-2}	3.44×10^{-2}	2.21×10^{-1}	6.41×10^{-1}	2.44×10^{-1}	5.54×10^{-1}
2	9.28×10^{-1}	9.20×10^{-1}	0	0	0	0
4	2.62×10^{-3}	7.86×10^{-3}	3.09×10^{-1}	3.39×10^{-1}	7.49×10^{-2}	2.11×10^{-1}
6	2.45×10^{-2}	2.72×10^{-2}	2.26×10^{-2}	3.01×10^{-3}	2.56×10^{-1}	2.07×10^{-1}
8	4.78×10^{-3}	6.19×10^{-3}	1.35×10^{-1}	1.57×10^{-2}	1.01×10^{-1}	8.42×10^{-3}
10	2.50×10^{-3}	2.85×10^{-3}	2.50×10^{-1}	1.11×10^{-3}	3.23×10^{-2}	8.98×10^{-3}
12	7.86×10^{-4}	1.07×10^{-3}	2.83×10^{-2}	4.74×10^{-4}	2.03×10^{-1}	7.58×10^{-3}
14	2.92×10^{-4}	3.34×10^{-4}	2.37×10^{-2}	6.97×10^{-5}	6.81×10^{-3}	7.37×10^{-4}
16	2.34×10^{-4}	3.03×10^{-4}	6.90×10^{-3}	2.02×10^{-5}	2.86×10^{-2}	5.94×10^{-4}
18	5.77×10^{-5}	6.42×10^{-5}	2.49×10^{-3}	5.12×10^{-6}	3.94×10^{-2}	5.60×10^{-4}
20	5.06×10^{-5}	6.35×10^{-5}	8.43×10^{-4}	1.55×10^{-6}	4.78×10^{-3}	9.01×10^{-5}
22	2.10×10^{-5}	2.34×10^{-5}	3.00×10^{-4}	5.50×10^{-7}	4.84×10^{-3}	8.74×10^{-5}
24	1.56×10^{-5}	1.76×10^{-5}	9.57×10^{-5}	2.35×10^{-7}	4.15×10^{-3}	9.99×10^{-5}

function presents many local maxima and minima. Using supersymmetric potentials for the ground state provides a smooth density distribution with a maximum near $r_{\alpha\text{-}\alpha} \approx r_{\alpha\text{-}\alpha\alpha} \approx 3$ fm. This result is consistent with the microscopic triple-α description of ^{12}C, which succeeds in reproducing the low-energy spectrum and spectroscopic properties with an equilateral-triangle structure of size close to 3 fm [31].

Table II shows the weights of the different K components in the ^{6}He and ^{12}C wave functions. For ^{6}He, the $K=2$ component represents about 90% of the wave function. The projection and supersymmetry methods provide very similar results. For ^{12}C, the weights are spread over several K values. The $K=2$ component vanishes, as a consequence of the symmetry of the system.

D. Electromagnetic transition probabilities

Spectroscopic properties of ^{12}C are complemented by electromagnetic matrix elements, given in Table III. Information concerning the calculation in the hyperspherical frame is provided in Appendix B. As mentioned previously for the rms radii, the quadrupole moment of the 2^+ state and the $B(E2,2^+\rightarrow0^+)$ value do not significantly depend on the method adopted to remove forbidden states. The supersymmetric approach gives a slightly stronger deformation, but both methods provide results consistent with experiment. The difference is larger for the $B(E2,0_2^+\rightarrow2^+)$ value which is in both cases underestimated by the model. From these results we conclude that rms radii and $E2$ properties do not provide a definite distinction between the forbidden-state removal methods. Most likely, other properties probing the details of the wave function, are necessary. In this context, electromagnetic form factors might be more severe constraints.

TABLE III. Electromagnetic properties of ^{12}C with the renormalized potentials. The bracketed values are obtained with a three-body potential (see Sec. V B).

	Projection	Supersymmetry	Experiment [a]
$Q(2^+)(e.\mathrm{fm}^2)$	5.2 (4.6)	6.0 (6.3)	6 ± 3
$B(E2,2^+\rightarrow0_1^+)$ (Wu)	4.1 (2.2)	5.5 (5.9)	4.65 ± 0.26
$B(E2,0_2^+\rightarrow2^+)$ (Wu)	3.5 (3.3)	0.9 (1.0)	8.0 ± 1.1

[a]Reference [32].

V. ASYMPTOTIC PROPERTIES

A. Three-body potentials and wave functions

Many physical processes essentially rely on asymptotic properties of the wave functions (see, e.g., Ref. [33]). The present work offers a good opportunity to investigate these properties along with the asymptotic behavior related to a three-body potential. In Fig. 8 we present diagonal and nondiagonal potentials for the ^{6}He system. Calculations are done by using the projection technique, and for typical values of γK. The centrifugal term is not included. A striking feature is that the decrease of the diagonal part is very slow at large distance. As expected, most potentials decrease as $1/\rho^3$ [18]. Very large ρ values (typically $\rho>40$ fm) must be considered to have negligible contributions, if one compares with the low binding energy of ^{6}He. On the other hand, a similar property holds for the nondiagonal potentials that cannot be neglected for $\rho\leqslant40$ fm. This supports the conclusion that many K values must be considered to get a good accuracy [6]. The corresponding wave functions are given in Fig. 8 in a linear scale. As expected, the $K=2$ component is dominant. It represents 71% and 21% of the $S=0$ and $S=1$ wave functions, respectively (see Table II).

Let us discuss the asymptotic properties of the wave functions. When all potentials are negligible, Eq. (14) gives, for large ρ values,

$$\chi^{J\pi}_{\gamma K}(\rho)\rightarrow A^{J\pi}_{\gamma K}\rho^{1/2}K_{K+2}(\kappa\rho), \tag{47}$$

where κ is the wave number, $K_n(x)$ is a modified Bessel function of order n, and $A^{J\pi}_{\gamma K}$ is the amplitude of the wave function at large distances. Asymptotically $K_n(x)$ tends to

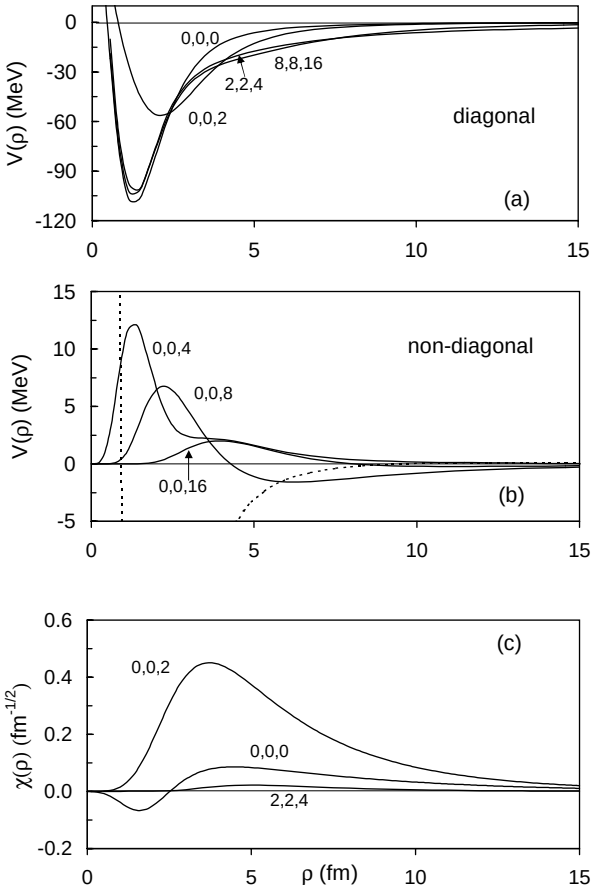

FIG. 8. (a) Diagonal potentials of ^{6}He (without the centrifugal term). The labels stand for (ℓ_x,ℓ_y,K). (b) Nondiagonal potentials; the curves correspond to the coupling with (0,0,0). The diagonal potential (0,0,0) (including the centrifugal term) is shown as a dotted line. (c) ^{6}He partial wave functions.

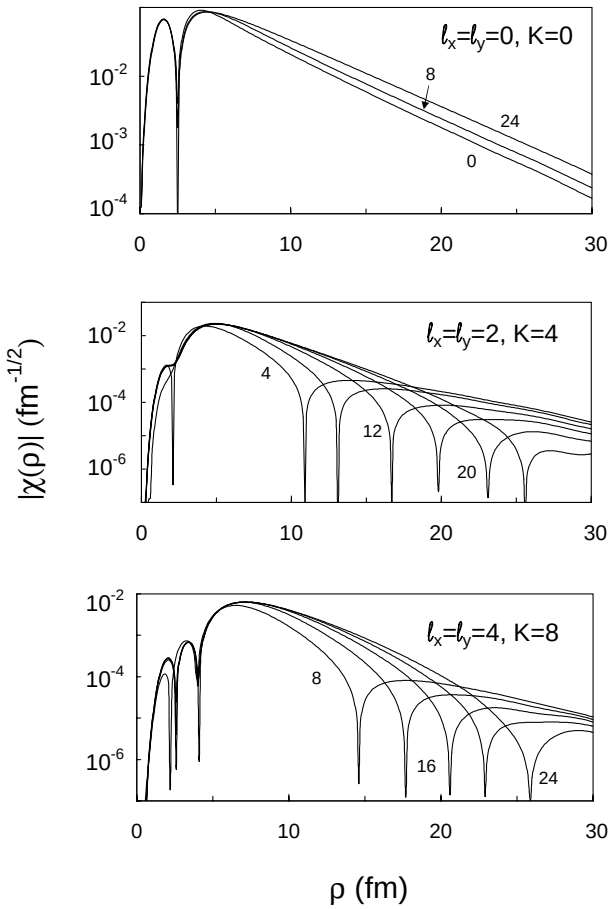

FIG. 9. Modulus of ^{6}He wave functions for different (ℓ_x,ℓ_y,K) values. The values of K_{max} are given as labels.

$$K_n(x)\to\sqrt{\pi/2x}\,\exp(-x). \tag{48}$$

In Fig. 9 we show the radial wave functions $\chi^{J\pi}_{\gamma K}(\rho)$ in a logarithmic scale, which provides more detail concerning the long-range part. For $\ell_x=\ell_y=0,2,4$, we have taken the component $n=0$ and repeated the calculation for several K_{max} values ($K_{max}=4$ to 24) by readjusting the strength of the potential in order to reproduce the experimental binding energy of ^{6}He. For $\ell_x=\ell_y=0$, the asymptotic behavior is almost linear in the logarithmic scale, as expected from Eqs. (47) and (48). The amplitudes $A^{J\pi}_{\gamma K}$ slightly depend on K_{max}. On the contrary, components with $\ell_x=\ell_y\neq 0$ behave in a different way. All these components present a node at large distance, beyond 10 fm. This node is pushed up to larger values as K_{max} increases, and tends to infinity. For lower values of K_{max} (say $K_{max}\leqslant 16$) the slope of the wave function between 5 and 20 fm is quite sensitive to K_{max}. Even with $K_{max}=24$ which provides the binding energy with an accuracy of 10^{-4} MeV, this external node plays a role. When ℓ_x and K_{max} increase, the accuracy of the long-range wave function requires even more basis functions. Of course these problems do not arise for the dominant $\ell_x=\ell_y=0$ terms in the wave functions. However, our numerical analysis shows that higher components require large K_{max} values to get a good accuracy on their asymptotic behavior. This property is not typical of the Lagrange-mesh method, and is expected to hold in any three-body method using hyperspherical coordinates. In particular, the supersymmetry approach presents the same behavior.

In order to go deeper in this analysis, we have calculated the wave functions in a Gaussian basis,

$$\chi^{J\pi}_{\gamma K}(\rho)=\rho^{K+5/2}\sum_{i=1}^{M} C^{J\pi}_{\gamma Ki}\exp(-\nu_i\rho^2), \tag{49}$$

where the width parameters ν_i are chosen in a geometric progression

$$1/\sqrt{\nu_i}=a_0x_0^{i-1}. \tag{50}$$

Of course, this method does not present the advantages of the Lagrange-mesh technique (see the discussion in Sec. IV B), but the differences with the Lagrange basis (37) would show up possible deficiencies in the long-range region. With typical values ($M=20$, $a_0=0.3$ fm, $x_0=1.3$), energies and wave functions are identical to those of Fig. 9 with a very high accuracy. In particular, the nodes observed in Fig. 9 are obtained at the same location. The wave functions with both bases are undistinguishable at the scale of Fig. 9.

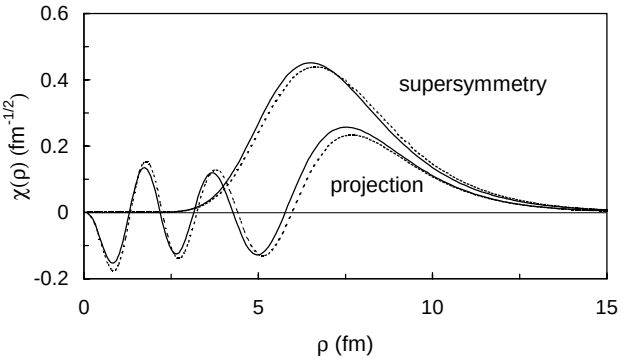

FIG. 10. ^{12}C radial wave functions for $\ell_x=\ell_y=K=0$. The full curves correspond to the renormalization of the α-α potential, and the dotted curves to the use of a three-body force.

B. Use of three-body forces

As discussed in Sec. IV, three-body calculations usually underestimate the binding energy if one uses original nucleus-nucleus potentials. The experimental energies have been reproduced by renormalizing the two-body interaction. This procedure is widely used in microscopic calculations where the force between free nucleons must be modified to account for the presence of other nucleons inside the nucleus; it provides effective forces that are adapted to several-nucleon systems. Renormalized nucleus-nucleus forces, however, modify two-body asymptotics. This is obvious here with the ^{12}C nucleus where ^{8}Be becomes bound with the renormalization factor required to reproduce the ^{12}C binding energy. For ^{6}He, this factor is quite close to unity, and the changes on the α-n phase shift are not significant. Another approach has been suggested by Fedorov and Jensen [17], who introduce a three-body force in the Hamiltonian, without modifying the original two-body interaction. The three-body force $V_{123}(\rho)$ is chosen as

$$V_{123}(\rho)=-\frac{V_3}{1+(\rho/\rho_3)^3}, \tag{51}$$

where ρ_3 is taken as 5 fm [18], and V_3 is fitted to reproduce the three-body binding energy.

For ^{6}He, the renormalization factor is $\lambda=1.0044$ or 1.027 according to the projection method (see Table I). Accordingly, very small V_3 values are needed ($V_3=0.2$ MeV and $V_3=0.1$ MeV, respectively). The changes in the wave functions are negligible. Since ^{12}C requires larger renormalization factors, V_3 is more important (see Ref. [17]): $V_3=19.3$ MeV with the projection method, and $V_3=23$ MeV with the supersymmetric method. The spectra are given as dotted lines in Fig. 5, and spectroscopic properties in Table III. Qualitatively, the energy spectrum is not different from the renormalization approach. Except for the $B(E2,2^+\rightarrow 0^+)$ value, the differences between the two procedures are less than 10%. This is confirmed by an analysis of the wave functions. In Fig. 10 we plot $\chi_{000}(\rho)$ for the ^{12}C ground state. As discussed previously, the projection method and the supersymmetric method provide very different wave functions, although spectroscopic properties are similar. Conversely, the introduction of a three-body force does not significantly affect the wave function, as soon as the binding energy is reproduced.

VI. CONCLUSION

In this work, we have used the Lagrange-mesh method to solve the three-body Schrödinger equation in hyperspherical coordinates. This method has been used in several other fields of nuclear and atomic physics, and is fast and accurate. Matrix elements of the potential do not require any integral over the hyper-radius, but a calculation of the potential value at the mesh points. In addition, the basis functions are orthogonal to each other, which strongly reduces numerical problems due to the accuracy of the method.

The technique has been applied to ^{6}He and ^{12}C, which are typical of weakly bound and strongly bound nuclei, respectively. We have addressed the problem of two-body forbidden states, which must be removed in the three-body calculation. The projection technique has been compared with the supersymmetric approach, by calculating rms radii, quadrupole moments and $E2$ transition probabilities in ^{12}C. These quantities do not enable us to discriminate between both the techniques. Other observables, such as electromagnetic form factors should help in probing the wave functions with more detail. With the original α-α potential of Buck *et al.* [23], the ground-state energy of ^{12}C is strongly underestimated. Introducing a renormalization factor is equivalent to using an effective α-α potential and provides realistic results for spectroscopic properties.

In a numerical point of view the projection method requires high accuracy as exemplified in Sec. IV. This problem is not significant when the number of forbidden states is small, as in ^{6}He, but gets more important for a larger number of forbidden states. The treatment of heavier systems, such as $^{16}\mathrm{O}+\alpha+\alpha$, for example, involves many two-body forbidden states and is expected to raise important numerical problems due to the accuracy. In this respect, the supersymmetric approach is simpler since it avoids the projector.

The asymptotic behavior of the partial components presents some remarkable features. For $\ell_x=\ell_y=0$, it is consistent with the expected modified Bessel function. For other components, it systematically displays a node which moves to larger distances when K_{max} increases. This feature does not depend on the basis, as exemplified by our second calculation with a Gaussian basis.

The Lagrange-mesh method also offers a good opportunity to investigate continuum three-body states [34]. To this end, the complex scaling method, limited to resonances, or the R-matrix method are ideal complements to the present study for the description of three-body continuum states.

ACKNOWLEDGMENTS

This text presents research results of the Belgian program P5/07 on interuniversity attraction poles initiated by the Belgian-state Federal Services for Scientific, Technical, and Cultural Affairs. P.D. acknowledges the support of the National Fund for Scientific Research (FNRS), Belgium.

APPENDIX A

In this appendix we provide some information about the calculation of matrix elements of the projector (42). In the basis, Eq. (40), the coupling scheme is $(\ell_x\ell_y)L(s_xs_y)SJ$, which is well adapted to the potential, but not to the operator (42). We denote the spins of particles 2 and 3 as s_x and s_y, respectively (we assume here that the core has a spin zero). Using usual transformation coefficients, we have

$$\langle\tilde{\Phi}^{JM\pi}_{\gamma Ki}(\boldsymbol{x},\boldsymbol{y})|\psi^{\ell sj}(x)Y^{\ell sjm}(\Omega_x)\rangle = \delta_{\ell\ell_x}\sum_{j_y}\langle jmj_yM-m|JM\rangle \times W(\ell,s,j,\ell_y,s_y,j_y,L,S,J) \times Y^{\ell_y s_y j_y m_y}(\Omega_y)\varphi^{J\pi}_{\gamma Ki,j}(y), \quad \text{(A1)}$$

where coefficients W and functions $\varphi^{J\pi}_{K\gamma i,j}(y)$ are obtained from

$$W(\ell_x,s_x,j_x,\ell_y,s_y,j_y,L,S,J) = [(2j_x+1)(2j_y+1)(2L+1) \times(2S+1)]^{1/2}\begin{Bmatrix}\ell_x & s_x & j_x\\ \ell_y & s_y & j_y\\ L & S & J\end{Bmatrix} \quad \text{(A2)}$$

and

$$\varphi^{J\pi}_{\gamma Ki,j}(y) = \mathcal{N}^{l_xl_y}_K\int_0^\infty \frac{x^{\ell_x+2}y^{\ell_y}}{(x^2+y^2)^{(\ell_x+\ell_y)/2}}P^{l_y+1/2,l_x+1/2}_n\left(\frac{x^2-y^2}{x^2+y^2}\right) \times\hat{f}_i\left(\frac{\sqrt{x^2+y^2}}{h}\right)\psi^{\ell sj}(x)dx. \quad \text{(A3)}$$

As mentioned in Sec. III C, two-body forbidden-states $\psi^{\ell sj}(x)$ are expanded over a Lagrange basis, and the Gauss approximation is used to evaluate this integral; we have

$$\varphi^{J\pi}_{\gamma Ki,j}(y) = \mathcal{N}^{l_xl_y}_K h_2^{1/2}\sum_{k=1}^{N_2}\lambda^{1/2}_{2k}D^{\ell sj}_k\frac{x_k^{\ell_x+2}y^{\ell_y}}{(x_k^2+y^2)^{(\ell_x+\ell_y)/2}} \times P^{l_y+1/2,l_x+1/2}_n\left(\frac{x_k^2-y^2}{x_k^2+y^2}\right)\hat{f}_i\left(\frac{\sqrt{x_k^2+y^2}}{h}\right) \quad \text{(A4)}$$

with $x_k=h_2u_k$. The use of Lagrange meshes therefore reduces this integral to a simple sum. Finally, the matrix element of the projector $P_{\ell j}$ is computed as

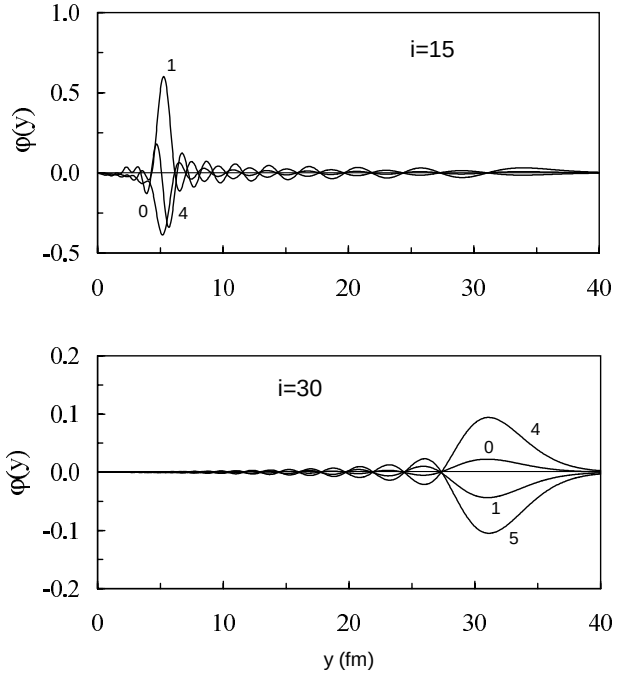

FIG. 11. Functions $\varphi^{0^+}(y)$ involved in the matrix elements of the forbidden-state projector [see Eq. (A4)]. The calculation is performed for ^{6}He, $\ell_x=\ell_y=S=0$, and for different n values (labels). Index i refers to the Lagrange function associated with the hyperradius.

$$\langle\tilde{\Phi}^{JM\pi}_{\gamma Ki}|P_{\ell j}|\tilde{\Phi}^{JM\pi}_{\gamma' K' i'}\rangle = \delta_{\ell\ell_x}\delta_{\ell\ell'_x}\delta_{\ell_y\ell'_y}\sum_{j_y}W(\ell,s,j,\ell_y,s_y,j_y,L',S',J) \times W(\ell,s,j,\ell_y,s_y,j_y,L,S,J) \times\int y^2\varphi^{J\pi}_{\gamma Ki,j}(y)\varphi^{J\pi}_{\gamma' K' i',j}(y)dy. \quad \text{(A5)}$$

The integral over y is evaluated numerically by using the trapeze method.

An example is shown in Fig. 11 where we present some functions $\varphi(y)$ involved in the calculation of the projector matrix elements [see Eqs. (A3) and (A4)]. The calculation is performed for ^{6}He, with $N=30$ and $h=0.3$ fm. The lower and upper panels correspond to Lagrange functions 30 and 15, respectively. These functions vanish at the 30 mesh points except one. This makes functions $\varphi(y)$ oscillating with a maximum, which is at large distances for high-order functions. This requires the α-α forbidden-states [$\psi^{\ell sj}(x)$ in Eq. (A3)] to be very accurate in a wide range.

APPENDIX B

In this appendix, we briefly describe the calculation of the electromagnetic matrix elements. For three particles, the electric and magnetic operators read

$$\mathcal{M}^E_{\lambda\mu}=e\sum_i^3 Z_i|\boldsymbol{r}_i-\boldsymbol{R}_{\rm c.m.}|^\lambda Y^\mu_\lambda(\Omega_{r_i-R_{\rm c.m.}}),$$

$$\mathcal{M}^M_{1\mu}=\sqrt{\frac{3}{4\pi}}\sum_i^3\left[\mu_N\frac{Z_i}{A_i}\ell_{i\mu}+\mu_i s_{i\mu}\right], \tag{B1}$$

where $\boldsymbol{R}_{\rm c.m.}$ is the center of mass coordinate, μ_N is the nuclear magneton ($\mu_N=e\hbar/2m_Nc$) and μ_i is the magnetic moment of particle i. For magnetic operators we limit ourselves to dipole components since, in practice, other multipolarities are not used.

By using Eq. (1), we have, for the electric operators ($Z_{23}=Z_2+Z_3, A_{23}=A_2+A_3$) as follows:

$$\begin{aligned}\mathcal{M}^E_{\lambda\mu}(\boldsymbol{x},\boldsymbol{y})=&e\left[Z_{23}\left(\frac{-A_1}{A}\right)^\lambda+Z_1\left(\frac{A_{23}}{A}\right)^\lambda\right]\mathcal{M}^E_{\lambda\mu}(\boldsymbol{y})\\&+e\left[Z_2\left(\frac{-A_3}{A_{23}}\right)^\lambda+Z_3\left(\frac{A_2}{A_{23}}\right)^\lambda\right]\mathcal{M}^E_{\lambda\mu}(\boldsymbol{x})\\&+e\sum_{k>0}^{\lambda-1}\alpha_{\lambda k}\left(\frac{-A_1}{A}\right)^k\left[Z_2\left(\frac{-A_3}{A_{23}}\right)^{\lambda-k}\right.\\&\left.+Z_3\left(\frac{A_2}{A_{23}}\right)^{\lambda-k}\right][\mathcal{M}^E_{k\mu}(\boldsymbol{y})\otimes\mathcal{M}^E_{\lambda-k\mu}(\boldsymbol{x})]^{\lambda\mu},\end{aligned} \tag{B2}$$

where the relative operators are defined as

$$\mathcal{M}^E_{\lambda\mu}(\boldsymbol{x})=\left(\frac{x}{\sqrt{\mu_{23}}}\right)^\lambda Y^\mu_\lambda(\Omega_x),$$

$$\mathcal{M}^E_{\lambda\mu}(\boldsymbol{y})=\left(\frac{y}{\sqrt{\mu_{(23)1}}}\right)^\lambda Y^\mu_\lambda(\Omega_y), \tag{B3}$$

and constant $\alpha_{\lambda k}$ reads

$$\alpha_{\lambda k}=\left[\frac{4\pi(2\lambda+1)!}{(2k+1)!(2\lambda-2k+1)!}\right]^{1/2}. \tag{B4}$$

If the external particles are identical, matrix elements involving crossed terms vanish for $\lambda=2$, and only the first two terms of the right-hand side of Eq. (B2) remain.

A similar calculation for the $M1$ operator provides

$$\begin{aligned}\mathcal{M}^M_{1\mu}(\boldsymbol{x},\boldsymbol{y})=&\sqrt{\frac{3}{4\pi}}\left\{\mu_N\frac{Z_{23}A_1^2+Z_1A_{23}^2}{AA_{23}A_1}\ell_{x,\mu}\right.\\&+\mu_N\frac{Z_2A_3^2+Z_3A_2^2}{A_2A_3A_{23}}\ell_{y,\mu}+\mu_N\sqrt{\frac{A_1A_2A_3}{A_{23}^2A}}\left(\frac{Z_2}{A_2}\right.\\&\left.\left.-\frac{Z_3}{A_3}\right)(\boldsymbol{x}\times\boldsymbol{p}_y+\boldsymbol{y}\times\boldsymbol{p}_x)_\mu+\sum_i\mu_i s_{i\mu}\right\},\end{aligned} \tag{B5}$$

where $\boldsymbol{p}_x$ and $\boldsymbol{p}_y$ are the momenta associated with $\boldsymbol{x}$ and $\boldsymbol{y}$.

The matrix elements of these operators between basis functions are calculated as described in Sec. II B. Integration over (Ω_x,Ω_y) is performed analytically, and integration over the hyperangle is performed numerically. Owing to the Gauss approximation, integration over the hyper-radius is trivial.

[1] P.M. Morse and H. Feshbach, *Methods in Theoretical Physics* (McGraw-Hill, New York, 1953), Vol. II.
[2] L.M. Delves, Nucl. Phys. **9**, 391 (1959).
[3] F.T. Smith, Phys. Rev. **120**, 1058 (1960).
[4] F.T. Smith, J. Math. Phys. **3**, 735 (1962).
[5] C.D. Lin, Phys. Rep. **257**, 1 (1995).
[6] R. Krivec, Few-Body Syst. **25**, 199 (1998).
[7] M.V. Zhukov, B.V. Danilin, D.V. Fedorov, J.M. Bang, I.J. Thompson, and J.S. Vaagen, Phys. Rep. **231**, 151 (1993).
[8] M. Fabre de la Ripelle, Ann. Phys. (N.Y.) **147**, 281 (1983).
[9] J. Raynal and J. Revai, Nuovo Cimento A **39**, 612 (1970).
[10] D. Baye and P.-H. Heenen, J. Phys. A **19**, 2041 (1986).
[11] M. Vincke, L. Malegat, and D. Baye, J. Phys. B **26**, 811 (1993).
[12] D. Baye, J. Phys. B **28**, 4399 (1995).
[13] D. Baye, Nucl. Phys. **A627**, 305 (1997).
[14] D. Baye, M. Hesse, and M. Vincke, Phys. Rev. E **65**, 026701 (2002).
[15] R. Tamagaki and Y. Fujiwara, Suppl. Prog. Theor. Phys. **61**, 229 (1977).
[16] P. Descouvemont and D. Baye, Phys. Rev. C **36**, 54 (1987).
[17] D.V. Fedorov and A.S. Jensen, Phys. Lett. B **389**, 631 (1996).
[18] I.J. Thompson, B.V. Danilin, V.D. Efros, J.S. Vaagen, J.M. Bang, and M.V. Zhukov, Phys. Rev. C **61**, 024318 (2000).
[19] D.R. Tilley, H.R. Weller, and G.M. Hale, Nucl. Phys. **A541**, 1 (1992).
[20] F.M. Nunes, J.A. Christley, I.J. Thompson, R.C. Johnson, and V.D. Efros, Nucl. Phys. **A609**, 43 (1996).
[21] M.C. Abramowitz and I.A. Stegun, *Handbook of Mathematical Functions* (Dover, New York, 1970).
[22] K. Wildermuth and Y.C. Tang, in *A Unified Theory of the Nucleus*, edited by K. Wildermuth and P. Kramer (Vieweg, Braunschweig, 1977).
[23] B. Buck, H. Friedrich, and C. Wheatley, Nucl. Phys. **A275**, 246 (1977).
[24] V.I. Kukulin and V.N. Pomerantsev, Ann. Phys. (N.Y.) **111**, 330 (1978).
[25] D. Baye, Phys. Rev. Lett. **58**, 2738 (1987).
[26] H. Kanada, T. Kaneko, S. Nagata, and M. Nomoto, Prog. Theor. Phys. **61**, 1327 (1979).
[27] D.R. Thompson, M. LeMere, and Y.C. Tang, Nucl. Phys. **A286**, 53 (1977).
[28] E.M. Tursunov, J. Phys. G **27**, 1381 (2001).
[29] E. M. Tursunov, D. Baye, and P. Descouvemont, Nucl. Phys. A (in press).

[30] V.T. Voronchev, V.I. Kukulin, V.M. Krasnopolsky, and P.B. Sazonov, Yad. Fiz. **43**, 1149 (1986).
[31] M. Dufour and P. Descouvemont, Nucl. Phys. **A605**, 160 (1996).
[32] F. Ajzenberg-Selove, Nucl. Phys. **A506**, 1 (1990).
[33] C. Forssén, V.D. Efros, and M.V. Zhukov, Nucl. Phys. **A697**, 639 (2002).
[34] B.V. Danilin, I.J. Thompson, M.V. Zhukov, and J.S. Vaagen, Nucl. Phys. **A632**, 383 (1998).